PCCP

ROYAL SOCIETY OF CHEMISTRY

PAPER

View Article Online
View Journal | View Issue

Cite this: *Phys. Chem. Chem. Phys.*, 2020, **22**, 7516

Chirality of a rhodamine heterodimer linked to a DNA scaffold: an experimental and computational study†

P. S. Rukin, ‡[a] K. G. Komarova, §*[a] B. Fresch, [b] E. Collini [b] and F. Remacle [a]

The chiroptical properties of multi-chromophoric systems are governed by the intermolecular arrangement of the monomeric units. We report on a computational and experimental study of the linear optical properties and supramolecular structure of a rhodamine heterodimer assembled on a DNA scaffold. The experimental absorption and circular dichroism (CD) profiles confirm the dimer formation. Computationally, starting from low-cost DFT/TDDFT simulations of the bare dimer we attribute the measured −/+ CD sign sequence of the S_1/S_2 bands to a specific chiral conformation of the heterodimer. In the monomers, as typical for rhodamine dyes, the electric transition dipole of the lowest π–π^* transition is parallel to the long axis of the xanthene planes. We show that in the heterodimer the sign sequence of the two CD bands is related to the orientation of these long axes. To account explicitly for environment effects, we use molecular dynamics (MD) simulations for characterizing the supramolecular structure of the two optical isomers tethered on DNA. Average absorption and CD-profiles were modeled using *ab initio* TDDFT calculations at the geometries sampled along a few nanosecond MD run. The absorption profiles computed for both optical isomers are in good agreement with the experimental absorption spectrum and do not allow one to discriminate between them. The computed averaged CD profiles provide the orientation of monomers in the enantiomer that is dominant under the experimental conditions.

Received 14th January 2020,
Accepted 9th March 2020

DOI: 10.1039/d0cp00223b

rsc.li/pccp

Introduction

Van der Waals π stacking complexes of organic chromophores have received a lot of attention as promising charge/energy transfer units in biological or bio-inspired non-covalent light-harvesting systems. Their functional optical properties strongly correlate with the spatial arrangement of the monomers that can be designed through an assembly procedure. Information about supramolecular structures available from X-ray crystallography data is not always fully relevant for systems in solution. In multi-chromophoric complexes, electronic circular dichroism (CD) spectroscopy serves as an efficient probe[1–10] of the arrangement of the monomeric units. In such complexes the Cotton effect, the characteristic change in sign of the CD bands, reflects the absolute arrangement of the respective transition dipole moments, which is governed by the relative orientation of the monomers.[11,12] For example, combined analysis of the spectral shift in the absorption spectrum with the sign-sequence in the CD spectra helps to clearly identify H-type or J-type aggregates[1,5,13–16] or to characterize the configuration of conjugated polymers.[17]

We previously investigated both experimentally and computationally at the QM/MM level the dynamics of coherent excitation in a model system engineered to mimic non-covalent light-harvesting complexes.[18] The photo-active component in this system is a heterodimer composed of the carboxytetramethylrhodamine (TAMRA) and sulphorhodamine (RHO) dyes. The two rhodamines are tethered on the 3′ and 5′ ends of suitably designed DNA strands by aliphatic linkers. When the formation of the double helix is promoted, these linkers ensure short distances in a range 3–6 Å (FWHM) between the two dye moieties, see Fig. 1 and Fig. S1 in the ESI.† The formation of a strongly coupled H-type heterodimer is confirmed by the experimental absorption and CD spectra (Fig. 1(d) and (e)).[18] The maximum in the absorption spectrum is blue-shifted as compared to the

[a] *Theoretical Physical Chemistry, UR MolSys B6c, University of Liege, B4000, Liege, Belgium. E-mail: kgvladi@fh.huji.ac.il*
[b] *Department of Chemical Sciences, University of Padova, via Marzolo 1, 35131 Padova, Italy*

† Electronic supplementary information (ESI) available. See DOI: 10.1039/d0cp00223b

‡ Present address: Federal Scientific Research Center "Crystallography and Photonics" Photochemistry Center, Russian Academy of Sciences, ul. Novatorov 7a, Moscow, 119421, Russian Federation.

§ Present address: The Fritz Haber Center for Molecular Dynamics, The Institute of Chemistry, Safra Campus, The Hebrew University of Jerusalem, Jerusalem 91904, Israel.

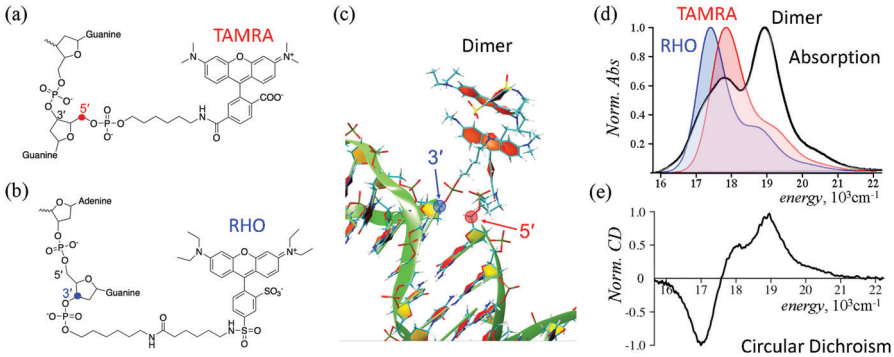

Fig. 1 (a–c) Structure of the supramolecular complex and (d, e) its optical response. Chemical structures of the TAMRA (a) and RHO (b) chromophores and their aliphatic linkers to the DNA nucleotides. (c) Zoom of the DNA double helix linking the chromophores. RHO is bound to the 3′ end of the DNA strand, while TAMRA is bound to the neighboring 5′ end (shown as blue and red circles). The 3′–5′ distance is 2.6 Å, which leads to a range of 3–6 Å (FWHM) for the dimer, see details in Fig. S1 (ESI†). (d and e) Experimental absorption and circular dichroism spectra of the supramolecular complex (c) in water (normalized to the maxima). In panel (d) the absorption spectra of the RHO–DNA (blue) and TAMRA–DNA (red) complexes are shown for comparison with the spectrum of the dimer. More details on the experimental procedures can be found in Section S1 of the ESI.†

spectra of the monomers (Fig. 1(d)) and the two optical bands have opposite signs in the CD spectrum (Fig. 1(e)).

The aggregation of dyes in solution is largely driven by thermodynamics. The balance between the solvation energy and the binding energy of the dimer determines the probability of the self-assembly of the monomeric units. In contrast, in the DNA–dye complex under study here, where the chromophores are covalently linked to the DNA scaffold, the stability of the conformers of the dimer is governed by multiple factors such as the DNA folding process and the steric hindrance between the chromophores, the linkers and the nuclear bases. As CD spectra are sensitive to the relative orientation of the monomers in the dimer, the investigation of the Cotton effect in this supramolecular complex provides important information about the structural arrangement of the chromophore units.

The experimental CD spectrum of the supramolecular complex, Fig. 1(e), points to a dominant orientation of the two monomers in the dimer tethered on the DNA fragment. In order to provide insights on the role of the orientation of the two chromophores of the dimer in the supramolecular complex, we explicitly simulate the effects of the DNA-backbone on the dimer initial conformations by building an ensemble of the ground state geometries.[19–25] To do so, we sample geometries along molecular dynamics (MD) trajectories of the whole system: the chromophore dimer linked to the DNA scaffold in water solution. For a given conformational space, we build the average absorption and CD lineshapes by computing the absorption and CD spectra of each sampled geometry *via* first principles electronic structure computation at the time-dependent density functional theory (TDDFT) level.[21,26–29] Specific interactions[22,26,30–32] of the chromophores with solvent water molecules are taken into account explicitly by including the first solvation shell within 2.5 Å in the TDDFT computation. Analysis of the MD trajectories shows primarily solvation of the carboxy- and sulfo-groups in TAMRA and RHO, respectively, see Section S3 of the ESI† for more details. The polarizable continuum model (PCM)[33] is then used to describe the water solvation effects on the electronic structure of this water–heterodimer complex.

The absorption spectrum of the H-type heterodimer formed by the RHO and TAMRA chromophores exhibits two close in energy peaks in the UV-visible region separated by 1100 cm^{-1} (Fig. 1(d)). QM/MM *ab initio* simulations[18] of the dimer allow us to relate these peaks to two π–π^* electronic transitions. Changes in the geometry of the dimer such as torsional motion in the chains of the linkers and variation in their relative orientation occur during the course of the MD trajectory due to the flexible nature of the aliphatic linkers. Such changes[34,35] alter the effective coupling between the dyes, and therefore affect the optical response (see discussion in the ESI,† Section S4).

Guided by the Kasha model of molecular dimers,[34] we characterize the relative motion of the RHO and TAMRA subunits using three intermolecular angles. The angle α between the long axes of the monomers, Fig. 2(a), describes the scissor-like motion of the subunits along the short axes of the xanthene moieties. The angle θ between the RHO long axis and the line connecting the molecular centers in the RHO → TAMRA direction, Fig. 2(b), shows the in-plane shift along the long axes of the xanthenes. In the Kasha approximation for the coupling between the two subunits these two angles play a major role. In addition, we monitor the change in the out-of-plane π stacking coplanar geometry of the xanthene moieties. To form a dimer, rather short distances (3–5 Å, see Fig. S1 in the ESI†) between the monomeric centers must be realized so that

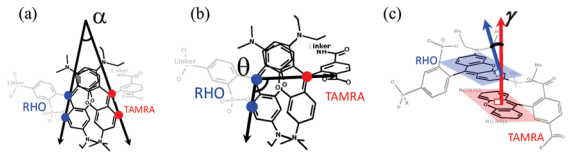

Fig. 2 Intermolecular angles of the dimer. We use these angles to characterize the relative orientation of the RHO and TAMRA subunits in the heterodimer. (a) The angle, α, between the long axes of the monomers; (b) the angle, θ, between the long axis of RHO and the line connecting the molecular centers in the RHO → TAMRA direction; and (c) the angle, γ, between the normal vectors to the RHO and TAMRA xanthene planes (shown as red and blue arrows).

exchange interaction can be significant. To characterize π stacking, we use the angle γ between the two normal vectors to the xanthene planes of TAMRA and RHO, Fig. 2(c) (see the details of the definition of γ in Section S4 of the ESI†). Using these three intermolecular angles we can examine and compare the relative position of the subunits along the MD trajectory.

In our previous work[18] we reported on *ab initio* simulations of the geometry and absorption spectrum of a dimer tethered on DNA described with QM/MM computations. In the present work we show that depending on the orientation of the monomeric units in the dimer, there can be two enantiomers of the RHO–TAMRA dimer. These optical isomers have different CD spectra but have very similar absorption spectra. We examine the distribution of the intermolecular angles during the MD trajectories in the chiral dimers and characterize the effects on their absorption and CD spectrum. Comparison with the experimental CD spectrum (Fig. 1(e)) therefore allows identifying the dominant orientation of the monomers in the dimer assembled during the double helix formation and the linking procedure for the two dyes. The analysis of the structures generated during room temperature MD shows that one of the enantiomers is destabilized by internal strains caused by the relative positions of the linkers tethering the chromophores to the DNA scaffold, thus explaining the net CD signal experimentally detected.

Computational details

The optical properties of the bare heterodimers are computed at the TDDFT/CAM-B3LYP-D level for the equilibrium ground state geometry of each enantiomer. Equilibrium geometries are obtained *via* DFT/CAM-B3LYP-D[36,37] calculations with the effects of the water solvent taken into account at the PCM level.[33] Such a model does not describe the explicit influence of the linkers and DNA environment, however it provides qualitative information on the chromophore properties in a polar medium. This level of modeling allows us to characterize the two enantiomers of the RHO–TAMRA bare heterodimer, which have similar absorption spectra and opposite sign sequences in the CD bands. All DFT/TD-DFT calculations are carried out using the 6-311G(d,p)[38–41] basis set within the Gaussian09 package.[42]

The conformational space of the supramolecular complex RHO–TAMRA tethered on a DNA strand is sampled from MD trajectories. The trajectories are calculated starting from the monomer orientation specific to each enantiomer, see Fig. S1 of the ESI† for a full structure of the supramolecular complex. We use the PARM99/BSC0 force field[43] for the atoms of the DNA strands and the TIP3P water model[44] for solvation. The force field for the chromophores and aliphatic linkers has been set-up within Antechamber using the GAFF force field parameters.[45] The initial geometry of the DNA duplex is built in B-DNA form using the NAB program.[46] As in the synthetic procedure the dyes are covalently linked to the DNA nucleotides *via* C6- and C12-aliphatic linkers, see Fig. 1. The supramolecular complex is solvated in a cubic periodic box with a minimum distance of 10 Å between DNA or chromophore atoms and the nearest box edge, see Fig. S2 in the ESI.† Sodium counter-ions are added to maintain the charge neutrality of the system. The system was optimized with the conjugate gradient and steepest descent methods to enable the relaxation of the initial solvation shells. After minimization and equilibration at a constant temperature (*NVT* Langevin temperature control, 300 K), a 150 ps simulation at a constant pressure (*NPT* ensemble) was run to achieve the proper density. The long-range electrostatic interactions were calculated using the particle mesh Ewald summation method[47] with a real-space cut-off distance of 9 Å. The SHAKE algorithm[48] was used to constrain bond vibrations involving hydrogen atoms. The time-step was set to 1 fs. All the MD calculations are performed within the AMBER12 program package.[49]

The rather high computational cost of the TDDFT calculations restricts the affordable number of sampled structures to a few hundreds of snapshots. Starting from the MD trajectories for each of the enantiomers tethered on DNA we compute excited state energies and oscillator and rotatory strengths for the 4 lowest transitions in configurations taken sequentially each 10 ps (400 samples for each optical isomer). For each sample only the chromophores with linkers and the nearest water molecules within a distance from the dye <2.5 Å are retained in the TDDFT/PCM calculations. The 2.5 Å threshold distance for the close contacts with the water molecules that are included in the TDDFT computation is determined from the analysis of the MD trajectory (for the details of the analysis see Section S3 of the ESI†).

We characterize the transitions from the ground to each excited electronic state using natural transition orbital (NTO) analysis[21,27,50] of the TDDFT transition density. From the coefficients of the atomic orbitals involved in each NTO we determine whether the orbital is localized on RHO, TAMRA or delocalized over both units. This allows us to group excited states by their character: localized on RHO or TAMRA, delocalized over the two units or RHO–TAMRA charge transfer states. The results of these computations are used to build the averaged absorption and CD profiles, see details in Section S5 of the ESI.†

Results and discussion

Spectroscopic properties of the optical isomers of the bare heterodimer in solution

We begin by analyzing the spectra at the equilibrium geometry of the two possible enantiomers at the TDDFT/CAM-B3LYP-D level of theory. The structure and spectra of the bare dimers in a water solution are simulated using PCM[33] to account for solvation effects.

The electric transition dipoles for the two lowest excited states in the RHO–TAMRA heterodimer are aligned with the long axes of the monomeric unit on which the transition is localized. The lowest S_0–S_1 transition is largely localized on the RHO unit and the electric transition dipole is parallel to the

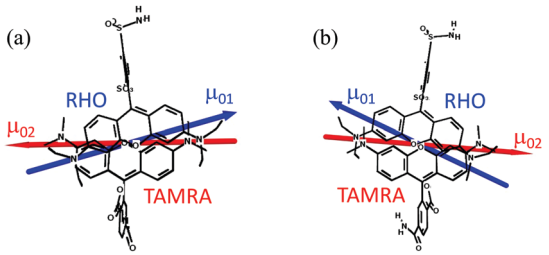

Fig. 3 Optical isomers of the heterodimer. Vectors of electric transition dipoles μ for the S_0–S_1 (blue arrows) and S_0–S_2 (red arrows) transitions for the chiral conformations D (a) and ch-D (b) in the bare heterodimer in solution. The vectors of the magnetic transition dipoles are collinear with the short axis of the xanthene plane (see Fig. S5 in the ESI†). The sign of the rotatory strength for the S_0–S_1 transition for D is positive, while for the ch-D orientation it is negative. The sign of the rotatory strength for the S_0–S_2 transition is opposite to that of S_0–S_1, leading to an opposite sign sequence in the CD spectra of the two enantiomers, see details in Table S1 of the ESI.†

direction of the RHO long axis. The second S_0–S_2 transition is mainly characterized by excitation on TAMRA, and its dipole is sensitive to its orientation with respect to RHO. This correlation allows us to construct a pair of chiral dimers, D and ch-D, where the 'ch' prefix stands for the 'chiral' form, see Fig. 3. The electric transition dipoles in these two enantiomers are oriented as a mirror image of one another. As the two structures differ only slightly for the two orientations of the units, the computed energy difference of the bare conformers is less than 1 kcal mol^{-1}. The quantum chemical simulation of the rotatory strengths of the S_0–S_1 and S_0–S_2 transitions indeed shows opposite signs of the CD bands in the D and ch-D conformations (see Table S1 in the ESI†).

The two bare enantiomers are essentially numerically degenerate, therefore one would expect to have both of them present in solution. The covalent linking of the chromophores to the DNA scaffold restricts the interconversion because of the rather short length of the linkers and other steric effects. Neither the D- or ch-D dimer tethered on DNA interconverts for a 4 ns run of the MD trajectory at room temperature. The difference in the DNA-linker environment in the two enantiomers tethered on DNA lifts the degeneracy of the bare forms, destabilizing one more than the other. This result is in agreement with the experimental CD spectrum, Fig. 1(e), which shows a definite sign of the two bands, which suggests that one optical conformer is significantly more abundant than the other.

In order to get a realistic simulation of the spectra of the dimers tethered on DNA and to better understand the structural constraints favoring the presence of one enantiomer over the other, we build a conformational space for each enantiomer. We use MD trajectories of the entire supramolecular complex with an initial geometry of the chromophores in the D or ch-D specific orientation. We then obtain the absorption and CD lineshapes for each enantiomer by averaging the spectra computed over a set of MD snapshots. By sampling the geometries along the MD trajectory we can readily include the effects of the partial flexibility of the weakly coupled heterodimer such as torsional motion in the chains of the linkers, variation in the relative orientation of the units and proximity of the units to the DNA backbone. This approach allows us to simulate realistic absorption and CD spectra in very good agreement with the experimental ones.

Sampling the conformations of the dimer linked to a DNA scaffold

We characterize the conformations of the dimers along a 4 ns MD trajectory for each enantiomer by looking at the distribution of the intermolecular angles, Fig. 4. Samples are taken sequentially with a 2 ps step, giving in total 2000 structures for each enantiomer. The histograms are computed using a 2° bin size for all the angles.

The scissor-like motion of the chromophore subunits results in a broad distribution of the α angle in both enantiomers, see Fig. 4(a) and (d). The main contribution to the ensemble comes from the range of $\alpha \approx 12$–24° (Fig. 4(a)) for D and $\alpha \approx 16$–30° for ch-D (Fig. 4(d)). Smaller values of the α angle correspond to almost parallel xanthene moieties, while the larger values that appear as a tail in the distribution, $\alpha \approx 30$–60°, correspond to oblique ones. Shifts along the long axes of the xanthene moieties are characterized by the histogram of the θ angle, Fig. 4(b) and (e). The distribution is asymmetric with a maximum at around 110° and a shoulder at around 90° (Fig. 4(b) and (e)). Comparison of the distribution of the α and θ angles for D and ch-D shows a larger dispersion in ch-D. Following the Kasha model briefly described in Section S4 of the ESI,† the increase in the dispersion of these angles leads to a larger dispersion in the coupling strength between the monomeric subunits, see eqn S4 (ESI†), which results in broader bands in the absorption and CD spectrum. Comparison of the averaged lineshapes for the D- and ch-D-dimers confirms this correlation as we discuss below.

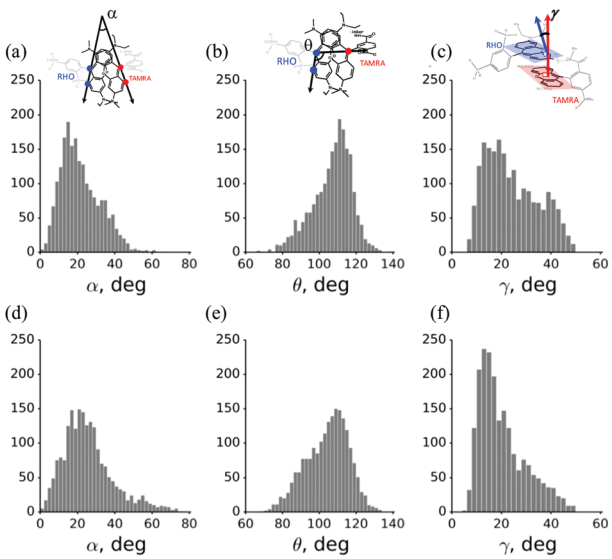

Fig. 4 Distribution of the intermolecular angles. The histogram for the α, θ and γ angles in the D (a–c) and ch-D (d–f) heterodimers tethered on DNA. See the definition of the angles in Fig. 2. Samples are taken sequentially along a 4 ns MD trajectory for each enantiomer with a 2 ps step (2000 structures).

The distribution of the γ angle, which characterizes deviations from the π stacking coplanar conformation of the dimer, has two components in both isomers: the main one located around $\gamma \approx 10$–24° and a tail that decays smoothly till almost 50°, Fig. 4(c) and (f). The major contribution of the smaller angles reflects a substantial exchange interaction between the units. The analysis of the MD trajectory of the D dimer shows a correlation of the intermolecular angles with the internal rotation of the voluminous ethyl-amino groups of RHO (Fig. S6 and S7 in Section S7 of the ESI†). In the MD snapshots when the RHO amino groups are both in *cis*-form outside the dimer subspace, Fig. S6b (ESI†), there is no steric hindrance between two monomeric units and coplanar conformers with small values of γ and α are observed. In the MD snapshots when one of the amino-groups is in the *trans*-configuration, Fig. S6c of the ESI,† the motion of TAMRA is restricted and parallel orientations of the monomers are not possible. Therefore, for these structures, if γ is small, providing good π stacking orientation, α is large (Fig. S7(e) and (i) of the ESI†). Such a *trans*-configuration of the ethyl-amino groups sterically restricts the relative motion of the two subunits and plays an important role in the dynamics and in the computed absorption and CD spectra.

Averaged absorption and CD lineshapes of the optical isomers tethered on DNA

The MD simulations at room temperature (300 K) capture various changes in the relative orientations of the monomers. These changes affect the coupling strength between the two chromophores and therefore the electronic structure of the excited states of the dimer. Moreover, the dynamics of the intermolecular modes coupled with the ethyl-amino group torsion in RHO governs the weights of different orientations in the ensemble. The consequences for the averaged optical response can be described only using explicit sampling of the configurational space of the dimer in its ground state.

The absorption profiles computed from averaging over the ensemble depend on the structures sampled during the MD trajectory and on the accuracy of the electronic structure calculations. Due to the large size of the dimer, QM/MM MD sampling[21,24,25,27] is not affordable. In the electronic structure calculations we use a TDDFT/PCM model as described above to compute the excited electronic states at geometries of the dimer taken from the snapshots from the MD trajectory (see an example of such a snapshot in Fig. S8 of the ESI†).

In the dimer there are localized excitations on each chromophore and partial charge-transfer excitations between them, which might be of importance in the description of the low-lying excited states.[35] We use the range-separated CAM-B3LYP functional to minimize the errors in the TDDFT description of the charge transfer states.[51] We expect that similar errors in the computation of excited electronic states are made only for the cases when the transitions have the same localization character. The two chromophores are from the same family of rhodamine dyes, and hence we assume that the local excitations in RHO and TAMRA are described with the same accuracy in TDDFT. We analyze the NTO involved in the 4 lowest transitions to characterize the electronic transitions and filter out from the ensemble samples that lead to a spurious electronic structure (see Section S10 of the ESI† for details). Because the NTOs are localized on each chromophore, see the NTOs for the two transitions in Fig. S9 of the ESI,† we use the weight, ω, of the main NTO of the transition as a measure of localization. This allows us to build the absorption profile separately for two groups: configurations with localized transitions where the main NTO has a weight $\omega > 0.8$ and delocalized transitions with $\omega < 0.8$. The first group forms the major contribution of the ensemble, 64% and 70% for D and ch-D, respectively. Delocalized transitions are found in 20% and 14.5% of samples in the D and ch-D ensemble. In these two groups the first transition is mainly localized on RHO, while the second transition is mainly localized on TAMRA, similar to the dimers studied in their equilibrium geometry.[18] The remaining 16–17% of samples have significantly different character of localization, therefore we do not include them in the averaging procedure, see a detailed description of this group in Section S10 in the ESI.†

The absorption and CD profiles for the D and ch-D enantiomers averaged over localized transitions are shown in Fig. 5 and Fig. S10–S13 of the ESI.† The partial contributions to the full absorption profile from the S_0–S_1 and S_0–S_2 transitions are highlighted as shaded areas of blue and red colour, respectively. The changes in the ground state geometry of the heterodimer result in the dispersion of the excitation energies and transition dipoles for both the S_0–S_1 and S_0–S_2 transitions. The relative intensities of the absorption bands and the resulting lineshapes (dashed lines in Fig. 5(a) and (b)) are in very good agreement with the experimental profile.

Most of the D and ch-D structures in the group with localized transitions show a rather intense first band in the absorption profile. For the group of samples with delocalized

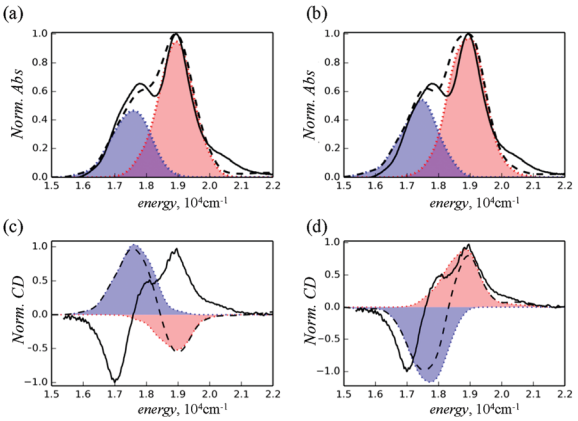

Fig. 5 Averaged absorption and CD spectra. Experimental (black solid line) and calculated (black dashed line) for samples of the D (a and c) and ch-D (b and d) isomers. The spectrum of the D isomer is averaged over 255 structures, and the one of the ch-D isomer over 280 samples. The partial contribution to the overall profile for the S_0–S_1 (blue) and S_0–S_2 profiles (red) is shown as shaded areas. The profiles are built up with same Gaussian broadening for all transitions. The intensity of each spectrum is scaled to its maximum. The calculated profiles are shifted down to the position of the experimental absorption maximum: -584 cm^{-1} and -713 cm^{-1} for the D and ch-D isomers, respectively.

transitions the S_0–S_1 band becomes almost dark, see Fig. S10 and S11(c), (d) in the ESI.† This is in agreement with the Kasha model, which predicts a fully dark lowest and a bright second excited state for an ideal dimer where the two eigenstates are fully delocalized. Such a correlation between the degree of localization of the NTO and the oscillator strength is also seen inside the group of localized transitions. Those structures which have weight of the RHO-localized NTO $\omega > 0.9$ lead to higher oscillator strengths for this transition (see Fig. S14, ESI†).

The comparison of the CD spectra for the D and ch-D optical isomers is shown in Fig. 5(c) and (d). We contrast the results of both computations with the experimental CD spectrum, where one can resolve two main peaks: a negative low-energy peak at 17 000 cm^{-1} and a positive one at around 19 000 cm^{-1} with a shoulder at 18 000 cm^{-1}. The computed CD spectra capture the two main peaks very well but not the shoulder. The more complicated lineshape in the experimental spectrum could be attributed to the mixture of the two enantiomers, or to a mixture of the relative orientations of the dimer influenced by the specific assembly path of the supramolecular complex. Nevertheless, the sign sequence of the CD bands in the experimental spectrum clearly corresponds to a dominant contribution of the ch-D enantiomer.

The relative stability of the two enantiomers is therefore strongly influenced by the environment composed of the linkers, the DNA scaffold and the solvent. An estimate of the free energy difference between the two enantiomers from our MD simulations is out of reach because of the importance of specific solvent–chromophore interactions and the impossibility of evaluating the entropic contribution with useful accuracy.[52,53] Nonetheless, a statistical analysis of the conformational space sampled by the MD trajectory of each isomer reveals that the D form is subjected to enhanced structural strains imposed by the configuration of the linker molecules.

In the case of the D enantiomer, the aliphatic linker of the RHO moiety can fold in proximity to the DNA backbone, Fig. 6(a). This is also seen from the comparison of the DNA–{RHO linker} distance distribution along the two MD trajectories, Fig. 6(c). One can see that the D-isomer remains closer to the DNA scaffold. It is characterized by restricted mobility compared to the ch-D form, as evidenced by the narrower distance distribution. The relative orientation of the two chromophores in the case of the ch-D form leaves the RHO linker in a less folded configuration which is not restricted by the DNA-strands, Fig. 6(b). The broader distribution of the DNA–{RHO linker} distance in the ch-D isomer suggests increased mobility of the {RHO linker} moiety in this isomer, likely associated with a favorable entropic gain in the free energy of the complex. The small portion of D-type structures for such a flexible conformation of the linker indicates that the length of the RHO linker is short enough to prevent significant isomerization into the D-form, see the illustration in Fig. S15 in the ESI.†

Destabilization of the chromophore in the D-dimer can be also seen indirectly from the distribution of the torsion angle of

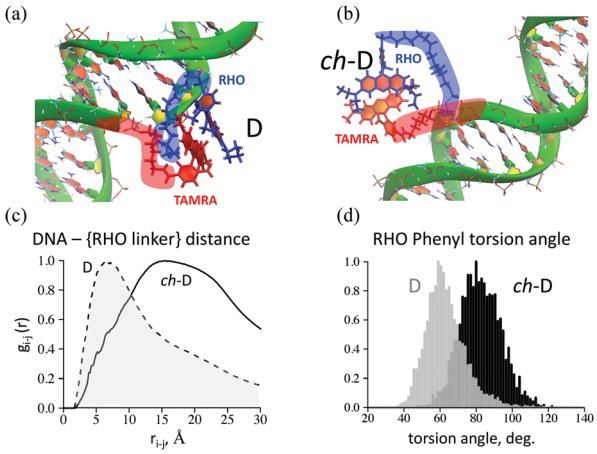

Fig. 6 Bent (a) and unfolded (b) conformation of the linkers in the two enantiomers tethered on DNA. Comparison of the configuration of the aliphatic linkers in the D (a) and ch-D (b) chromophores covalently linked to DNA. RHO and TAMRA chromophores are shown in blue and red colors, respectively. Each chromophore's linkers are highlighted with the same color code. (c) Radial distribution functions, $g_{i-j}(r)$, relating two interacting centers (i) and (j) for D (dashed line) and ch-D (solid line) optical isomers tethered on DNA. (i) Atoms of the DNA duplex and (j) atoms of the RHO aliphatic linker. (d) The histogram for the dihedral angle related to the torsion of the phenyl substituent in RHO for the two enantiomers: D – gray color, ch-D – black color. Each distribution is normalized to its maximum.

the RHO phenyl-substituent with respect to the xanthene moiety. The chromophore is anchored to the DNA by covalent linking to this phenyl-ring and therefore its relative orientation is sensitive to the strains due to the linker conformation.

The phenyl ring is almost perpendicular to the xanthene plane in the optimized bare dimer (with a dihedral angle of 83° for the ch-D dimer and 91° for the D-form), while it is perturbed by the strain imposed by the linker once the dimer is tethered to the scaffold. Comparison of the distribution of this angle along MD trajectories of the two enantiomers shows that in the D dimer the phenyl substituent is more perturbed than in the ch-D dimer, see Fig. 6(d). The mean value of the angle distribution is about 60° in the D-form, and about 80° in the ch-D-isomer, confirming an enhanced strain imposed on the D-form with subsequent destabilization of the D-complex. Such a difference in the DNA-linker environment of the two enantiomers tethered on DNA lifts the degeneracy of the bare forms and dictates the chirality of the whole complex.

Conclusions

In this work, we model the structural and optical properties of the RHO–TAMRA heterodimer tethered on a DNA scaffold. We characterize the effect of the environment on the relative orientation of the two chromophores, on the electronic properties of the heterodimer and on the corresponding absorption and CD spectra by sampling geometries along a MD trajectory. We identified and characterized two enantiomers, D and ch-D, that can contribute to the experimental CD spectrum. Starting from the bare dimers in solution we relate the sign sequence of the CD

spectra to the angle between the long axes of the xanthene moieties of RHO and TAMRA. The optical isomers of the bare dimers are almost degenerate, and therefore both can be present in solution. Tethering of the dimer on the DNA scaffold through aliphatic linkers leads to specific steric hindrance that lifts the degeneracy of the bare enantiomers. Comparison between experimental CD spectra and the computed spectra averaged over the MD sampled geometries allows us to identify that ch-D is the dominant enantiomer formed under the experimental conditions. Our joint experimental and computational study suggests that specific chiroptical properties of heterodimers can be induced by a complex environment and assembly procedure.

Conflicts of interest

There are no conflicts to declare.

Acknowledgements

We thank Prof. I. Willner from the Hebrew University of Jerusalem for providing the samples of the dimers tethered on DNA. This work was supported by the EC FET project COPAC #766563 and the Fonds National de la Recherche Scientifique (F.R.S-FNRS, Belgium) #T.0205.20 and #J.0012.18. PR thanks the Ministry of Science and Higher Education within the State assignment FSRC ''Crystallography and Photonics'' RAS (Project No. AAAA-A19-119040490079-8) in part ''Sampling the conformations of the dimer linked to DNA scaffold'' and the Russian Science Foundation (Project No. 19-13-00383) in part ''Averaged absorption and CD lineshapes of the optical isomers tethered on DNA'' for their support. B. F. acknowledges the support of the Italian Ministero dell'Istruzione, Università e Ricerca through the grant Rita Levi Montalcini – 2013. FR is supported by F.R.S.-FNRS.

Notes and references

1 B. L. Cannon, L. K. Patten, D. L. Kellis, P. H. Davis, J. Lee, E. Graugnard, B. Yurke and W. B. Knowlton, *J. Phys. Chem. A*, 2018, **122**, 2086–2095.
2 B. L. Cannon, D. L. Kellis, L. K. Patten, P. H. Davis, J. Lee, E. Graugnard, B. Yurke and W. B. Knowlton, *J. Phys. Chem. A*, 2017, **121**, 6905–6916.
3 F. Nicoli, M. K. Roos, E. A. Hemmig, M. Di Antonio, R. de Vivie-Riedle and T. Liedl, *J. Phys. Chem. A*, 2016, **120**, 9941–9947.
4 D. G. Singleton, R. Hussain, G. Siligardi, P. Kumar, P. J. Hrdlicka, N. Berova and E. Stulz, *Org. Biomol. Chem.*, 2016, **14**, 149–157.
5 G. Pescitelli, L. Di Bari and N. Berova, *Chem. Soc. Rev.*, 2014, **43**, 5211–5233.
6 N. Berova, L. D. Bari and G. Pescitelli, *Chem. Soc. Rev.*, 2007, **36**, 914–931.
7 M. Balaz, B. C. Li, J. D. Steinkruger, G. A. Ellestad, K. Nakanishi and N. Berova, *Org. Biomol. Chem.*, 2006, **4**, 1865–1867.
8 F. Segatta, L. Cupellini, M. Garavelli and B. Mennucci, *Chem. Rev.*, 2019, **119**, 9361–9380.
9 D. Padula, S. Jurinovich, L. Di Bari and B. Mennucci, *Chem. – Eur. J.*, 2016, **22**, 17011–17019.
10 H. Gattuso, A. Spinello, A. Terenzi, X. Assfeld, G. Barone and A. Monari, *J. Phys. Chem. B*, 2016, **120**, 3113–3121.
11 W. W. Parson, *Modern Optical Spectroscopy*, Springer, Heidelberg, 2007.
12 J. A. Schellman, *Chem. Rev.*, 1975, **75**, 323–331.
13 F. C. Spano, *J. Am. Chem. Soc.*, 2009, **131**, 4267–4278.
14 T. Brixner, R. Hildner, J. Köhler, C. Lambert and F. Würthner, *Adv. Energy Mater.*, 2017, **7**, 1700236.
15 R. S. Stoll, N. Severin, J. P. Rabe and S. Hecht, *Adv. Mater.*, 2006, **18**, 1271–1275.
16 L. I. Markova, V. L. Malinovskii, L. D. Patsenker and R. Häner, *Chem. Commun.*, 2013, **49**, 5298–5300.
17 K. Watanabe, Z. Sun and K. Akagi, *Chem. Mater.*, 2015, **27**, 2895–2902.
18 M. Cipolloni, B. Fresch, I. Occhiuto, P. Rukin, K. G. Komarova, A. Cecconello, I. Willner, R. D. Levine, F. Remacle and E. Collini, *Phys. Chem. Chem. Phys.*, 2017, **19**, 23043–23051.
19 R. Szabla, H. Kruse, P. Stadlbauer, J. Sponer and A. L. Sobolewski, *Chem. Sci.*, 2018, **9**, 3131–3140.
20 D. Fazzi, M. Barbatti and W. Thiel, *J. Phys. Chem. Lett.*, 2017, **8**, 4727–4734.
21 J. J. Nogueira, F. Plasser and L. Gonzalez, *Chem. Sci.*, 2017, **8**, 5682–5691.
22 V. A. Spata, W. Lee and S. Matsika, *J. Phys. Chem. Lett.*, 2016, **7**, 976–984.
23 W. Arbelo-Gonzalez, R. Crespo-Otero and M. Barbatti, *J. Chem. Theory Comput.*, 2016, **12**, 5037–5049.
24 V. A. Spata and S. Matsika, *Phys. Chem. Chem. Phys.*, 2015, **17**, 31073–31083.
25 C. M. Isborn, A. W. Götz, M. A. Clark, R. C. Walker and T. J. Martínez, *J. Chem. Theory Comput.*, 2012, **8**, 5092–5106.
26 R. Crespo-Otero and M. Barbatti, *Theor. Chem. Acc.*, 2012, **131**, 1237.
27 V. A. Spata and S. Matsika, *J. Phys. Chem. A*, 2014, **118**, 12021–12030.
28 M. Barbatti and K. Sen, *Int. J. Quantum Chem.*, 2016, **116**, 762–771.
29 N. De Mitri, S. Monti, G. Prampolini and V. Barone, *J. Chem. Theory Comput.*, 2013, **9**, 4507–4516.
30 P. V. Komarov and V. G. Plotnikov, *Int. J. Quantum Chem.*, 2012, **112**, 3039–3045.
31 K. G. Komarova, S. N. Sakipov, V. G. Plotnikov and M. V. Alfimov, *J. Lumin.*, 2015, **164**, 57–63.
32 A. V. Marenich, C. J. Cramer and D. G. Truhlar, *J. Phys. Chem. B*, 2015, **119**, 958–967.
33 J. Tomasi, B. Mennucci and R. Cammi, *Chem. Rev.*, 2005, **105**, 2999–3094.
34 M. Kasha, H. R. Rawls and M. Ashraf El-Bayoumi, *Pure Appl. Chem.*, 1965, **11**, 371–392.

35 N. J. Hestand and F. C. Spano, *Chem. Rev.*, 2018, **118**, 7069–7163.
36 T. Yanai, D. P. Tew and N. C. Handy, *Chem. Phys. Lett.*, 2004, **393**, 51–57.
37 G. Stefan, E. Stephan and G. Lars, *J. Comput. Chem.*, 2011, **32**, 1456–1465.
38 R. Krishnan, J. S. Binkley, R. Seeger and J. A. Pople, *J. Chem. Phys.*, 1980, **72**, 650–654.
39 M. M. Francl, W. J. Pietro, W. J. Hehre, J. S. Binkley, M. S. Gordon, D. J. DeFrees and J. A. Pople, *J. Chem. Phys.*, 1982, **77**, 3654–3665.
40 D. Feller, *J. Comput. Chem.*, 1996, **17**, 1571–1586.
41 K. L. Schuchardt, B. T. Didier, T. Elsethagen, L. Sun, V. Gurumoorthi, J. Chase, J. Li and T. L. Windus, *J. Chem. Inf. Model.*, 2007, **47**, 1045–1052.
42 M. J. Frisch, G. W. Trucks, H. B. Schlegel, G. E. Scuseria, M. A. Robb, J. R. Cheeseman, G. Scalmani, V. Barone, B. Mennucci, G. A. Petersson, H. Nakatsuji, M. Caricato, X. Li, H. P. Hratchian, A. F. Izmaylov, J. Bloino, G. Zheng, J. L. Sonnenberg, M. Hada, M. Ehara, K. Toyota, R. Fukuda, J. Hasegawa, M. Ishida, T. Nakajima, Y. Honda, O. Kitao, H. Nakai, T. Vreven, J. A. Montgomery, Jr., J. E. Peralta, F. Ogliaro, M. Bearpark, J. J. Heyd, E. Brothers, K. N. Kudin, V. N. Staroverov, R. Kobayashi, J. Normand, K. Raghavachari, A. Rendell, J. C. Burant, S. S. Iyengar, J. Tomasi, M. Cossi, N. Rega, J. M. Millam, M. Klene, J. E. Knox, J. B. Cross, V. Bakken, C. Adamo, J. Jaramillo, R. Gomperts, R. E. Stratmann, O. Yazyev, A. J. Austin, R. Cammi, C. Pomelli, J. W. Ochterski, R. L. Martin, K. Morokuma, V. G. Zakrzewski, G. A. Voth, P. Salvador, J. J. Dannenberg, S. Dapprich, A. D. Daniels, Ö. Farkas, J. B. Foresman, J. V. Ortiz, J. Cioslowski and D. J. Fox, *Gaussian 09, Revision D.01*, 2009.
43 A. Pérez, I. Marchán, D. Svozil, J. Sponer, T. E. Cheatham, C. A. Laughton and M. Orozco, *Biophys. J.*, 2007, **92**, 3817–3829.
44 W. L. Jorgensen, J. Chandrasekhar, J. D. Madura, R. W. Impey and M. L. Klein, *J. Chem. Phys.*, 1983, **79**, 926–935.
45 J. Wang, R. M. Wolf, J. W. Caldwell, P. A. Kollman and D. A. Case, *J. Comput. Chem.*, 2004, **25**, 1157–1174.
46 T. J. Macke and D. A. Case, *Molecular Modeling of Nucleic Acids*, American Chemical Society, 1997, ch. 24, vol. 682, pp. 379–393.
47 T. Darden, D. York and L. Pedersen, *J. Chem. Phys.*, 1993, **98**, 10089–10092.
48 S. Miyamoto and P. A. Kollman, *J. Comput. Chem.*, 1992, **13**, 952–962.
49 D. A. Case, T. A. Darden, T. E. Cheatham, C. L. Simmerling, J. Wang, R. E. Duke, R. Luo, R. C. Walker, W. Zhang, K. M. Merz, B. Roberts, S. Hayik, A. Roitberg, G. Seabra, J. Swails, A. W. Gotz, I. Kolossváry, K. F. Wong, F. Paesani, J. Vanicek, R. M. Wolf, J. Liu, X. Wu, S. R. Brozell, T. Steinbrecher, H. Gohlke, Q. Cai, X. Ye, J. Wang, M.-J. Hsieh, G. Cui, D. R. Roe, D. H. Mathews, M. G. Seetin, R. Salomon-Ferrer, C. Sagui, V. Babin, T. Luchko, S. Gusarov, A. Kovalenko and P. A. Kollman, *AMBER 12*, 2012.
50 R. L. Martin, *J. Chem. Phys.*, 2003, **118**, 4775–4777.
51 M. J. G. Peach, P. Benfield, T. Helgaker and D. J. Tozer, *J. Chem. Phys.*, 2008, **128**, 044118.
52 B. Fresch and F. Remacle, *Phys. Chem. Chem. Phys.*, 2014, **16**, 14070–14082.
53 A. Pohorille, C. Jarzynski and C. Chipot, *J. Phys. Chem. B*, 2010, **114**, 10235–10253.